CONF-950624--1

LBL-37481
UC-404

Lawrence Berkeley Laboratory
UNIVERSITY OF CALIFORNIA

Materials Sciences Division

Presented at the International School of Physics "Enrico Fermi" Workshop on the Chemical Physics of Fullerenes 10 (5) Years Later, Varenna, Italy, June 6–17, 1995, and to be published in the Proceedings

Theoretical Study of the Structure and Electronic Properties of Carbon and $B_XC_YN_Z$ Nanotubes

S.G. Louie

June 1995

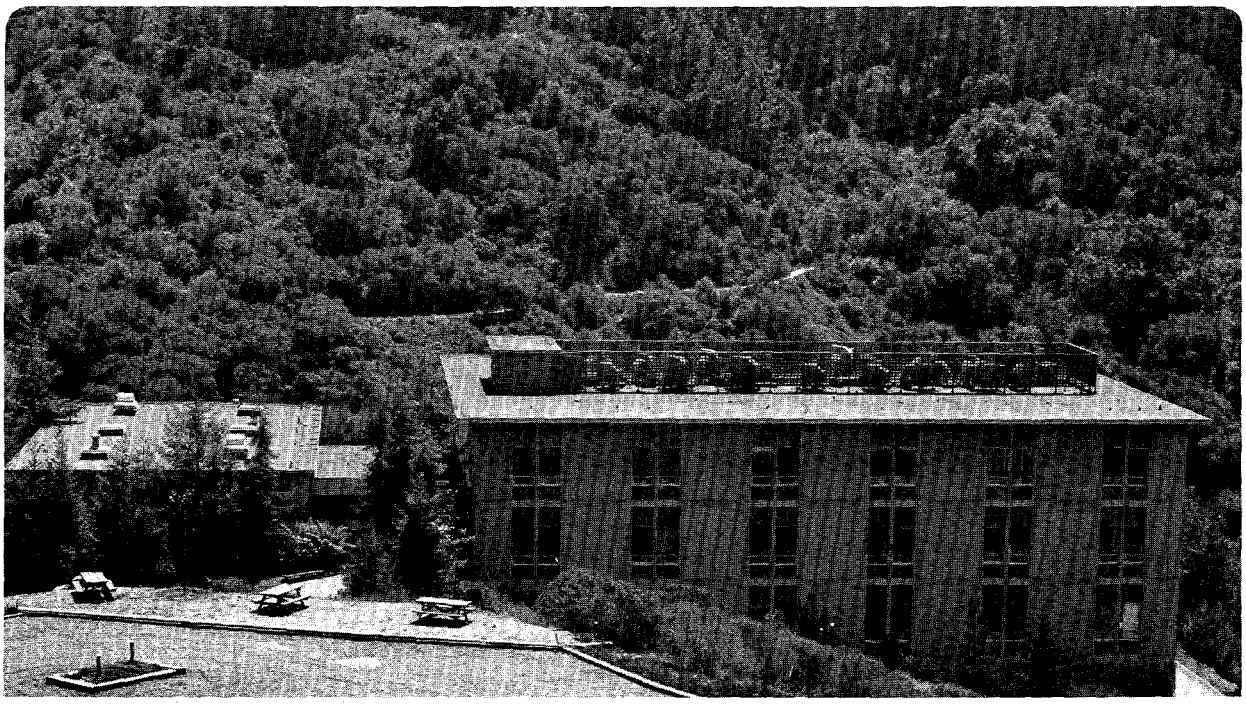

Prepared for the U.S. Department of Energy under Contract Number DE-AC03-76SF00098

DISCLAIMER

Portions of this document may be illegible in electronic image products. Images are produced from the best available original document.

LBL-37481
UC-404

Theoretical Study of the Structure and Electronic Properties of Carbon and $B_XC_YN_Z$ Nanotubes

Steven G. Louie

Department of Physics
University of California

and

Materials Sciences Division
Lawrence Berkeley Laboratory
University of California
Berkeley, California 94720

June 1995

This work was supported by National Science Foundation Grant No. DMR95-20554 and by the U.S. Department of Energy under Contract No. DE-AC03-76SF00098.

LBL-37481
UC-404

To appear in the Proceedings of the International School of Physics "Enrico Fermi" Workshop on the Chemical Physics of Fullerenes 10 (5) Years Later.

THEORETICAL STUDY OF THE STRUCTURE AND ELECTRONIC PROPERTIES OF CARBON AND $B_XC_YN_Z$ NANOTUBES

STEVEN G. LOUIE
Department of Physics
University of California at Berkeley
and
Materials Sciences Division
Lawrence Berkeley Laboratory
Berkeley, CA 94720

Abstract

Theoretical studies of the electronic and structural properties of carbon nanotubes and nanotubes composed of boron, carbon and nitrogen are presented. Structural stability, hybridization effects, static dielectric response, incorporation of metal atoms, and collapsed tube structures are calculated. Nanotubes of BN, BC_3, and BC_2N are predicted to form and have very different properties from those of the carbon systems. BN nanotubes are found to be constant band gap insulators with novel free-electron tubule states at the conduction band minimum. The possibility of chiral currents in doped BC_2N nanotubes is shown.

1. Introduction

It was just four years ago S. Iijima published his seminal paper reporting the discovery of the carbon nanotubes [1]. Over this relatively short period, nanotubes has become a highly active and rapidly growing field. Tremendous progress has been made in many fronts including means for high yield production of multi- and single-wall carbon nanotubes, incorporation of foreign atoms into the tubules, theoretical understanding of their structural, electronic and mechanical properties, prediction and synthesis of new classes of nanotubes involving noncarbon elements, and numerous possible applications of these novel materials.

In this article, we give a short review of some selected theoretical studies on the structural and electronic properties of nanotubes with emphasis on the prediction and understanding of the properties of small radius carbon nanotubes and nanotubes

composed of boron, carbon, and nitrogen atoms. The other articles in this Volume will undoubtedly cover the many other fascinating aspects of nanotubes.

The structure of the article is as follows. Carbon nanotubes are discussed in Section 2. Total energy results predict that the tubules are stable down to very small radii. Re-hybridization of the graphene network states is shown to be as important as band-folding effects in determining the metallicity of small radius tubules. Calculation of the static polarizability tensor of these tubules reveals a rather unique dependence on their electronic and geometric structures. The structure and properties of carbon tubules doped with alkali metals in the interior are also investigated. Although metallic K does not wet graphite, we show that very small diameter tubes do incorporate K atoms. Finally, a study of the recently observed collapsed carbon nanotubes (or nano-ribbons) is presented.

The B-C-N nanotubes are discussed in Section 3. We predict the formation of BN, BC_2N, and BC_3 tubules with strain energies which are in fact slightly more favorable than those of the carbon nanotubes. The BN nanotubes are predicted to be constant band gap materials, independent of their radius and helicity; and the conduction band minimum is composed of a novel "free-electron-tubule" state with wavefunction amplitude concentrated in the interior of the tube away from the tubule wall. The existence of chiral currents in these nanotubes, in particular for the BC_2N tubules, is explored.

Section 4 provides a summary and some conclusions.

2. Carbon Nanotubes

2.1 STABILITY, ELECTRONIC STRUCTURE, AND HYBRIDIZATION EFFECTS

In additional to the multi-wall carbon nanotubes originally reported by Iijima, single-wall tubules with a narrow distribution of diameters have been synthesized using arc discharge with transition metal catalysts [2]. In this subsection, we focus our discussion on the energetics and electronic structure of the small radius single-wall nanotubes [3]. Questions of particular interest are: 1) How does the tubule curvature affect the electronic states, and 2) what is the structural stability of the very small radius tubes?

Although there are still only few direct experimental data on these systems, the electronic structures of the carbon nanotubes have been predicted early to be highly unusual and sensitive to their geometric structures, varying from metals to semiconductors depending on size and chirality [4-6]. This prediction, verified by tight-binding calculations, results from the unique electronic structure of a single graphene sheet, which has a Fermi surface consisting only the six corner points of the hexagonal Brillouin zone, and a band-folding assumption that the tubule electronic bands near the Fermi energy E_F may be obtained from the π bands of a graphene sheet by applying the tubes' azimuthal periodic boundary conditions. This picture is expected to be valid for

large tubes. However, since tubules with radius as small as 3.5Å have been experimentally produced; hybridization between the π and σ states may be important.

Calculations [3] based on the *ab initio* pseudopotential local density functional (LDA) method indeed show that sufficiently strong hybridization effects do occur in the small radius tubules which significantly alter their electronic structure from those obtained in previous tight-binding calculations. Strongly modified low-lying conduction band states are introduced into the band gap of insulating tubes because of hybridization of the σ^* and π^* states. As a result, the LDA gaps of some tubes are lowered by more than 50%, and the (6,0) tube (in the notation of Saito et al [5]) which previously predicted to be semiconducting is shown to be metallic. The calculated band gaps of several selected nanotubes are given in Table I.

Table 1. Band gap (in eV) of selected carbon tubes. For the metallic case, the overlap of the bands is given as a negative gap

Tubes	TB	LDA
(6,0)	0.05	(-0.83)
(7,0)	1.04	0.09
(8,0)	1.19	0.62
(9,0)	0.07	0.17

Beside the dramatic change in the (6,0) tube, we see in Table I that within LDA the tubes (7,0) and (8,0) are semiconductors, consistent with tight-binding calculations, but with a much smaller gap. This discrepancy is due to the existence of a singly degenerate $\sigma^* - \pi^*$ rehybridized state which is much lower in energy in the LDA calculations than in the tight-binding work.

The LDA band structure and density of state (DOS) for the tube (6,0) are shown in Fig. 1. The state labeled (a) is the singly degenerate state mentioned above. At the Γ point, this state is 0.83 eV below the doubly degenerate state that forms the top of the valence band in tight-binding calculations. This band overlap makes the (6,0) tube a metal. In general, the discrepancy between tight-binding and LDA calculations decreases as the radius of the tubules increases. This is consistent with the fact that, in large tubes with small curvatures, the interaction between the σ and π bands become increasing negligible, and the nanotube band structure can be given with increasing accuracy by "folding" the graphite sheet band structure.

To illustrate the hybridization effect further, we show in Fig. 2 the charge density distribution for the state (a) at Γ for the tube (6,0). The wavefunction for this state is mostly localized outside the tube. If this state is π or π^* derived, it would have equal weight inside and outside the tube. Analysis of other (n,0) tubes also indicates that this

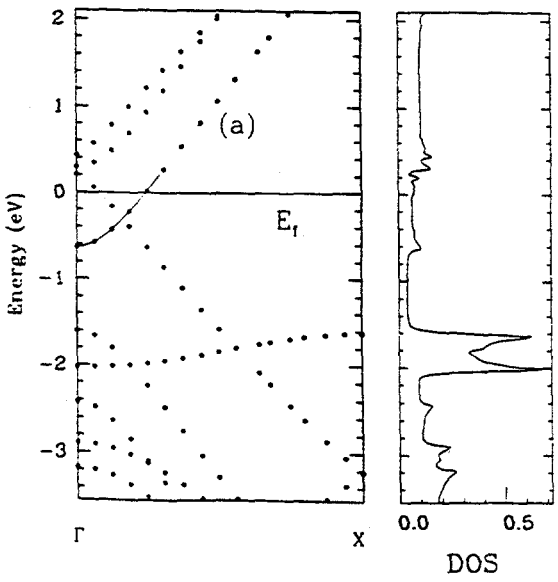

Fig. 1. Band structure and DOS of the carbon nanotube (6,0).

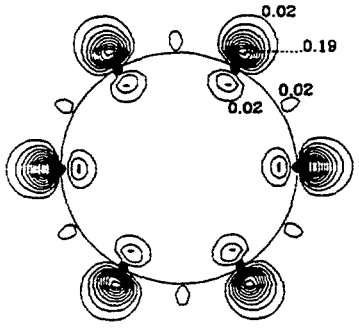

Fig. 2. Charge density of state (a) in Fig. 1.

state should be mostly outside of the tubes for k-vectors near the zone center. Thus, for the small radius tubes, $\sigma^* - \pi^*$ hybridization is as important as band-folding effects in determining the metallicity of small radius tubes.

In terms of stability, total energy LDA calculations[3] revealed that the carbon tubules are energetically stable with respect to strips down to quite small radii. Plotted in Fig. 3 is the calculated strained energy per atom (relative to the energy per atom of a graphene sheet) as a function of the diameter for several small tubules. The solid line is a fit, which scales as d^{-2} (where d is the diameter) as given by classical elasticity theory. Thus, for the strain energy of the tubules, the elasticity picture holds down to subnanometer scale. We shall use this relation later in our discussion of collapsed nanotubes. Also shown in Fig. 3 is the energy per atom (above that of a graphite sheet because of the dangling bonds on the edges) for the case of a (6,0) strip. As seen from the figure, strip formation is not favored since the energy/atom scales as d^{-1}. For example, for a (6,0) tube with diameter of d=4.78 Å, its calculated energy is lower by more than 0.2 eV/atom compared to that of the corresponding strip. The elastic energy in the tubule is still considerably lower than the dangling bond energy in forming the strips at d≈4 Å, in agreement with a previous classical force-field calculation [7].

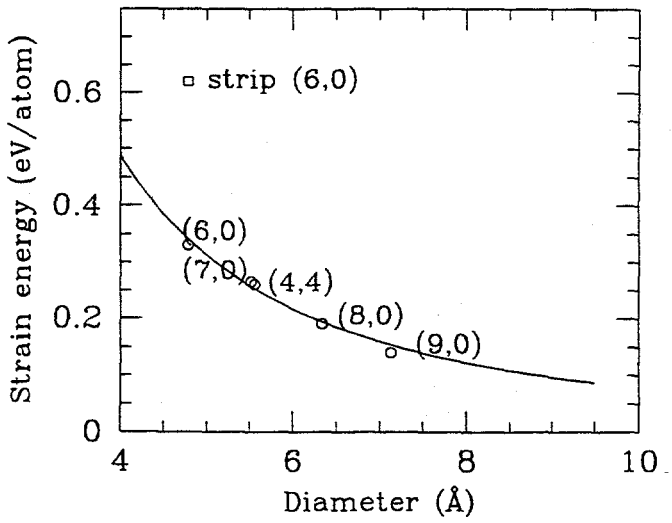

Fig. 3. Calculated strain energy/atom for carbon nanotubes

2.2 STATIC POLARIZABILITIES

Since the electronic structures of the carbon nanotubes are highly sensitive to their geometric structures, an interesting and importance issue is then the geometric dependence of the electric polarizabilities of such tubes. To explore this issue for a large number of carbon tubes of varying size and chirality, a tight-binding calculation for the static polarizabilities has been carried out for the case of a uniform applied electric field [8]. The unscreened polarizability α_O is calculated within the random phase approximation with basically one adjustable parameter fitted to the polarizability of C_{60} [9]. Because of the cylindrical symmetry of the tubes, the polarizability tensor may be divided into components perpendicular to the tube axis, $\alpha_{O\perp}$, and a component parallel to the axis, $\alpha_{O\|}$. Using arguments analogous to those used for C_{60} [10,11], local field corrections to the screened polarizability tensor may be included classically via the relations (for an infinitely long tube):

$$\alpha_\perp = \frac{\alpha_{O\perp}}{1 + \frac{2\alpha_{O\perp}}{R_{eff}^2}} \tag{1}$$

and

$$\alpha_\| = \alpha_{O\|} \tag{2}$$

where $R_{eff} = R+\delta R$ is an effective radius of the tube with $\delta R = 1.2$Å.

The calculated results for the unscreened polarizabilities $\alpha_{O\perp}$ and $\alpha_{O\|}$ as a function of the tube radius are presented in Figs. 4 and 5, respectively. The trends obtained are quite striking. Figure 4 is consisted of results from 17 different tubes with very different band gaps. The theory shows that $\alpha_{O\perp}$ is totally independent of the band gap E_g and is linearly proportional to the radius square. The latter may be understood from classical arguments; but the former is rather unexpected. The non dependence of the $\alpha_{O\perp}$ on E_g is basically a consequence of selection rules in the dipole matrix elements [8]. For a uniform electric field perpendicular to the tube axis, the symmetry of the electronic states dictates that the dipole matrix element between the highest occupied states and the lowest unoccupied states to be zero in the band-folding picture. This leads to the insensitive of the polarizability to the minimum gap of the electronic structure of the tubes. Figure 5, on the other hand, shows that $\alpha_{O\|}$ is proportional to R/E_g^2, which is consistent with the static dielectric response of standard insulators.

The effect of local fields, at least within the simple model given by Eqs. (1) and (2), is to saturate $\alpha_\perp$ for large $\alpha_{O\perp}$, but leave $\alpha_\|$ unaffected. The basic conclusion is then, in general, the polarizability tensor of a carbon nanotube will be highly anisotropic with $\alpha_\| \gg \alpha_\perp$.

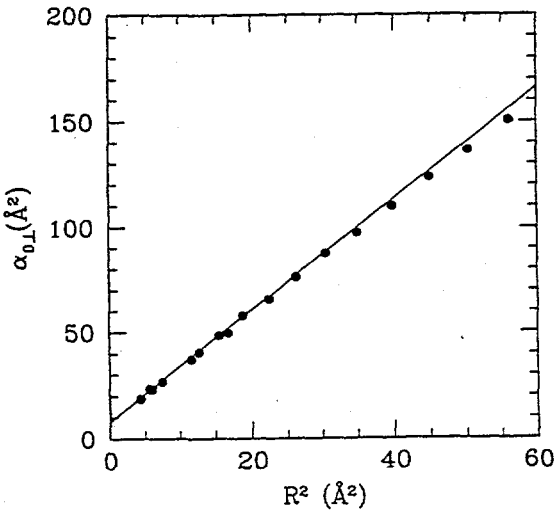

Fig. 4. Plot of $\alpha_{O\perp}$ versus R^2 for various carbon tubes.

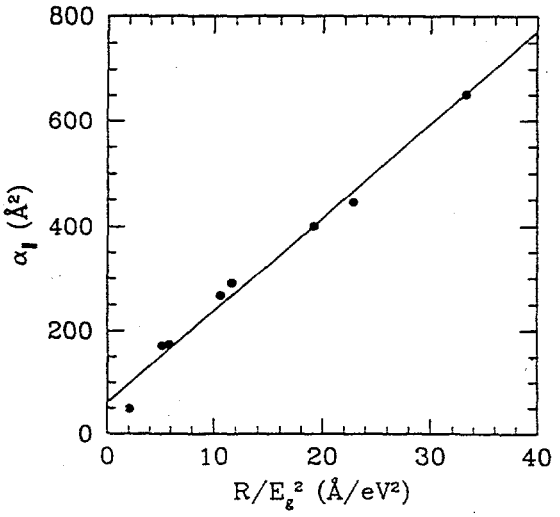

Fig. 5. Plot of $\alpha_{O\parallel}$ for various carbon nanotubes.

2.3 ALKALI METAL INCORPORATION

Capillary action of foreign atoms or molecules into carbon nanotubes have been studied theoretically and experimentally [12,13]. In particular, the encapturation of metals is of interest for the possible fabrication of nano-scaled wires. Because of confinement, metals inside tubules may form new phases which do not exist under other conditions, including the possibility of new superconductors. The surface tension of the liquid metals has been proposed as a key factor in determining whether capillary action (or wetting) occurs [14], with a threshold of 190mN/m or less for wetting. Using this criterion, K atoms would not be captured inside the carbon nanotubes while Rb atoms would.

Recent total energy calculations [15,16] for linearly-aligned arrangement of metal atoms in the nanotubes however showed that the classical wetting picture of capillary action may not be applicable on the subnanoscale. For example, in the case of K atom incorporation, it is found that exothermic cohesion does occur for tubules with diameters less than 1 nm. The calculated heat of formation can be greater than 1 eV per K atom depending on tubule diameters as shown in Table II. The most favorable diameter for cohesion is found to range from 5 to 6 Å. (The heat of formation is obtained by subtracting the energy of a K-doped tubule from the sum of the energies of the isolated systems of bulk K metal and an undoped tubule.)

Analysis of the electronic structure shows that the origin of the cohesion is one of an ionic interaction, with charge transfer of one electron from the K atom to the tubule conduction bands. Further, the energy barrier for sliding of K chain inside the tubules considered is found to be the same order of magnitude as that of K-diffusion in the graphite intercalation compounds [17,18]. Thus K intercalation into small radius tubes is expected to occur easily when vapor phase K is used as a source. Another interesting result is that, because the electrons of the K atoms are transferred to the tubule bands, the conductivities of these K-doped small tubules will be dominated by carriers on the tubule walls rather than on the K-chains.

Table II. Heats of formation E_h of the (n,0) tubules having K atoms inside.

Tubes	D(Å)	E_n (eV/K atom)
(6,0)	4.78	~ 0
(7,0)	5.56	1.12
(8,0)	6.34	1.07
(9,0)	7.13	0.30

2.4 COLLAPSED TUBULES: TWISTED RIBBON STRUCTURES

Carbon nanotubes are expected to be very strong along the axial direction because of the strength of the carbon-carbon bond. However, they may distort perpendicular to their axis. Indeed, nanotubes observed, either single- or multi-wall ones, are often far from perfect. Bends, folds, localized kinks, and other defects have been reported by various groups. An outstanding question has been whether or not a nanotube could ever suffer complete collapse along its length. Recent experimental observation using transmission electron microscopy confirmed that fully collapsed multiwall carbon nanotubes, i.e. nanoribbons, do occur quite naturally under appropriate conditions [19].

Theoretically, it is shown that for a given range of tube parameters, a completely collapsed tube is energetically favorable over the more familiar cylindrical nanotubes [19]. This behavior may be modeled using elasticity theory together with the van der Waals attraction between graphene sheets. The basic physics may be understood as follows. For a single-wall inflated tube, the energy per length (relative to the flat sheet) is given by

$$E_{tube} = \pi k/R, \tag{3}$$

where R is the radius and k the curvature modulus which may be obtained from total energy calculations [3]. However, for a fully collapsed single-wall tube with the opposite tubule walls at a van der Waals distance away from each other as shown in Fig. 6, the energy per length will be composed of a higher curvature energy due to the edges which is independent of the radius R and a negative van der Waals contribution from the interaction of the opposite faces of the wall, i.e.,

$$E_{ribbon} = \text{constant} - E_{vdw} \times (\pi R - a). \tag{4}$$

Since E_{ribbon} linearly decreases with R, at sufficiently large radius, the collapsed tube would have a lower energy than the inflated tube. We note that the constant corresponding to the edge curvature energy in Eq. (4) increases with the number of walls N on the tube. The critical radius $R_{crit}(N)$ over which the collapsed tube will be favored is an increasing function of N.

Using an experimentally determined value of $E_{vdw} = 0.02$ eV/Å^2 [20] and a curvature modulus k of 1.4 eV from LDA total energy calculations [3], we have performed a variational calculation for the cross-sectional shape and $R_{crit}(N)$ of the collapsed tubes. We found $R_{crit}(1) \approx 8d$ and $R_{crit}(8) \approx 19d$ where d is the van der Waal distance. Fig. 6(b) depicts the predicted cross section for an N=8 collapsed tube with radius $R = R_{crit}$. The outer width of this ribbon structure is 238Å which is slightly greater than but comparable to a measured width of ≈200Å for the N=8 collapsed tube observed experimentally [19].

The existence and stability of these new nanotube structures may have implication on their electric and mechanical properties. For example, the electronic structure of a

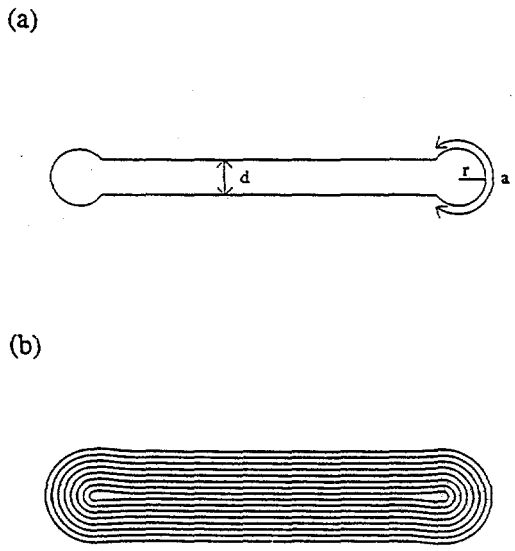

Fig. 6. (a) Schematic diagram of a single-wall collapsed tube. (b) Theoretically modeled 8-wall fully collapsed tube with $R=R_{crit}$.

collapsed carbon or other nanotube may be significantly different from the fully inflated structure. Mechanically, the bending of a ribbon is expected to be much easier than that of a cylindrical tube.

3. BN, BC_3, and BC_2N Nanotubes

Based on the similarities among graphite, hexagonal boron nitride, and various boron-carbon-nitrogen compounds, it is reasonable to expect that nanotubes composed of boron, carbon, and nitrogen would be stable. Specific B-C-N nanotubes have been predicted [21-25], and their synthesis achieved recently in experiments using various techniques [26-30]. The properties of this new class of nanotubes are calculated to be quite different from those of the carbon nanotubes.

3.1 ENERGETICS

In addition to hexagonal BN, the lesser known compounds of BC_3 and BC_2N [31,32] also crystallize into graphitic-sheet-like structures. LDA total energy calculations have predicted that tubules of all three compounds are stable [22-24]. The strain energy required to roll the sheets into tubules are found to be in fact smaller than

those of the carbon nanotubes. Figure 7 shows the calculated energy per atom for several BN tubes as a function of the tube diameter, with the zero of energy referred to the energy per atom of an isolated BN sheet. Also shown is the strain energy of the carbon nanotubes. As for the carbon tubes, the BN tube energies follow the classical $1/R^2$ strain law, where R is the radius of the tubes. The results clearly show that the strain energy of BN nanotubes is smaller than that of the carbon nanotubes. It is energetically less costly to form a BN nanotube than a carbon nanotube of the same radius. The energy of a strip is also given in Fig. 7. Since the strip energy is higher and it scales as 1/R, the BN nanotubes are stable with respect to the formation of strips for tubes with radius larger than 4Å. Calculations on BC_3 and BC_2N nanotubes have given very similar results. (See Fig. 8.)

An interesting structural difference between the carbon and BN nanotubes is that there is a significant structural relaxation for the small radius BN tubes [22]. The system buckles with the boron atoms moving inward and the nitrogen moving outward, resulting in a dipolar double cylinder shell structure. The distance between the inner B-cylinder and the outer N-cylinder is mostly independent of tube helicity, and decreases with increasing radius. The driving mechanism for this structural relaxation is attributed to the fact that B atoms like to form planar sp^2 bonds whereas N atoms prefer to be in a s^2p^3 environment.

3.2 ELECTRONIC PROPERTIES

Unlike a graphite sheet, a BN sheet is a wide-gap semiconductor with a band gap over 5.5 eV [25] and the BC_3 and BC_2N sheets are semiconductors [23,24]. The electronic band structure of the B-C-N nanotubes is therefore expected to be different from the carbon nanotubes which can lead to important differences in their properties and applications.

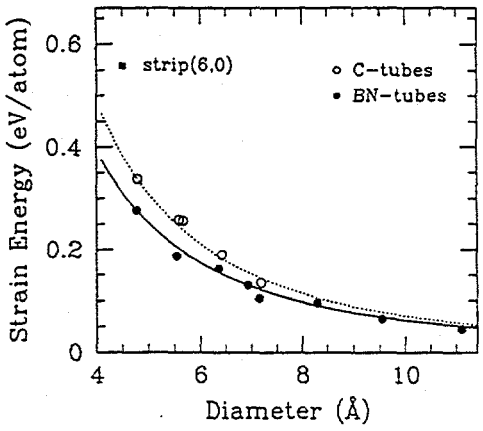

Fig. 7 Energy per atom for BN (dots) and carbon (open circle) nanotubes and that of a strip (filled square).

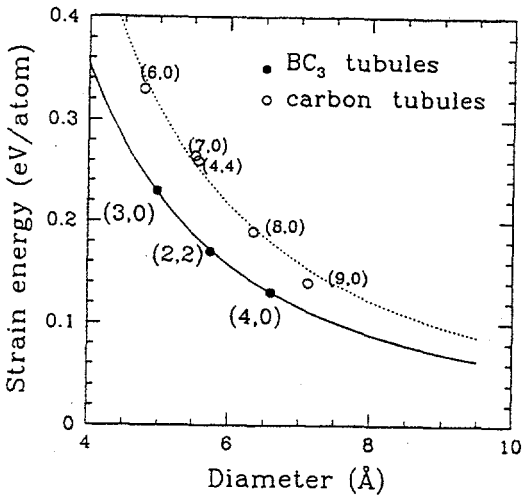

Fig. 8. Energy per atom for BC_3 (dots) and carbon (open circle) nanotubes.

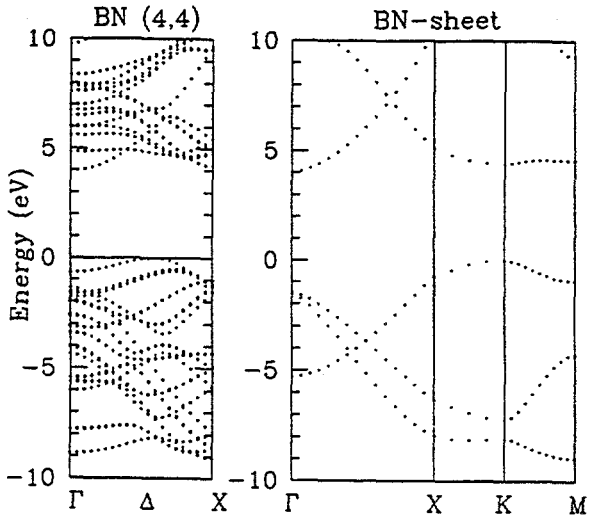

Fig. 9. Calculated LDA band structure of a (4,4) BN tube.

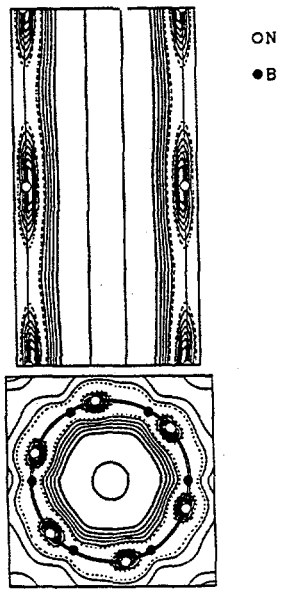

Fig. 10. Charge density plot of the CBM state of the (6,6) BN nanotube. a) A plane containing the tube axis and N atoms. b) A plane perpendicular to the tube axis containing B and N atoms

The BN nanotubes are predicted to be wide-gap insulators with $E_g \approx 5.5$ eV, independently of their radius and helicity [22]. Figure 9 depicts the calculated LDA band structure of a (4,4) BN tube together with the band structure of a BN sheet. Results from calculations on a number of tubes show that except for the smallest radius tubes the LDA band gap is pinned at the constant value of about 4 eV. Quasiparticle calculations [25] show that self-energy corrections [33] to the LDA open the gap to 5.5 eV. This large gap is a result of the large ionicity of this compound. The constancy of the BN tube band gap also holds for multi-wall tubes, and it may be of importance for technological applications because samples containing many different sizes and structures could be grown with predictable electronic properties.

The constant-gap value of the BN tubes is related a novel electronic state at the bottom of the conduction band. Unlike other states near the gap which are π-like, the conduction band minimum (CBM) for all BN tubes with radius larger than 5Å is made up of a highly unusual state. This is a state with carriers moving freely in the center of the tube. Figure 10 is a contour plot of the charge density corresponding to the CBM for the (6,6) BN nanotube. As seen from the figure, the maximum of the wavefunction is at the center of the tube, away from the atomic sites. The calculated effective mass of this band corresponds to the free electron mass. This free-electron tubule state persists even for the multi-wall structures. We thus expect the BN tubes to exhibit remarkable

properties under n-type doping. The free-electron state is originated from a "sheet" state of an isolated BN sheet. For a single BN sheet, the CBM is consisted of such a "free-electron" state, corresponding to an electron wavefunction very weakly bound to the BN sheet. Upon rolling the sheet into a tube, this sheet state wraps onto itself to form the free-electron tubule state.

Since both BC_3 and BC_2N are much less ionic than BN, their band gaps are significantly smaller. The free-electron tubule states in these systems are much higher in energy than the CBM (as in the case of carbon) and do not play an important role in their electronic properties. Single-wall BC_3 nanotubes are found to be semiconductors with $E_g \leq 0.5$ eV [23]. However, because of interaction between the walls, multi-wall BC_3 tubes are likely to be metals. Another characteristic feature of BC_3 is that, unlike carbon systems, the planar BC_3 sheet has both π and π^* bands above the Fermi level, and this feature is retained in the electronic structure of the BC_3 tubules. The calculated density of states of a single BC_3 sheet and that of the (2,2) tubule are depicted in Fig. 11. The two sharp peaks above E_F originated from the π and π^* bands are seen in both systems. In contrast, the lower of the two peaks would be below E_F in the DOS of the carbon nanotubes. The same double peak structure should be observed in multi-wall BC_3 tubes, making this feature characteristic of the BC_3 compounds.

Because of the anisotropic geometric structure of the BC_2N sheet [34], different chiral structures may be obtained by rolling the BC_2N sheets into tubes. Calculations

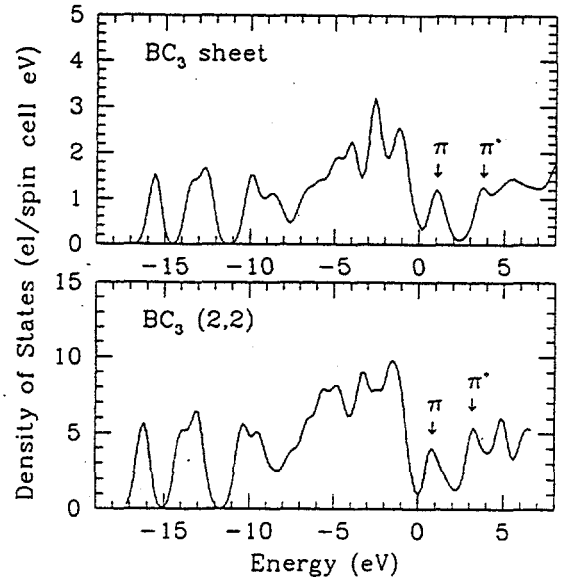

Fig. 11. Density of states of a BC_3 sheet (upper panel) and of a (2,2) tubule (lower panel) from LDA calculations.

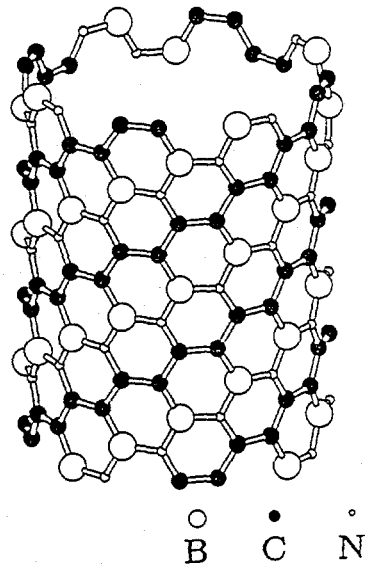

Fig. 12. Model of the BC_2N (4,4) nanotube. The vertical direction is the tubule axis. Some atoms on the back side are not shown for simplicity.

[24] have shown that the BC_2N tubules are generally semiconductors which can be doped with either acceptors or donors. Also, since the BC_2N sheets have anisotropic in-plane conductivity, helical currents may be produced in the appropriately doped chiral tubules making them nanoscale coils. Figure 12 shows a model of a BC_2N (4,4) tubule obtained by rolling a sheet with atomic positions determined from a total energy LDA calculation. Experimentally, it is known that a honeycomb structure exists for BC_2N sheet but the exact atomic structure has not been determined. Calculations based on a relaxation time Boltzmann formalism show that chiral currents do occur on either a p- or n-type doped (2,2) BC_2N nanotube [35].

4. Summary and Conclusions

We have given a short review of some theoretical studies of the structural and electronic properties of carbon nanotubes and nanotubes composed of boron, carbon and nitrogen. Theory shows that nanotubes are stable down to very small radius where hybridization effects can become important in determining the electronic structure of these systems. The static dielectric responses of the carbon nanotubes are found to be highly anisotropic in general. Incorporation of K atoms is found favorable for appropriate diameter tubes. The newly observed phenomenon of collapsed nanotubes is explained in

terms of a competition between positive curvature energy and negative van der Waals interactions. BN, BC_3, and BC_2N nanotubes are predicted to form and have strikingly different properties from those of the carbon nanotubes. We find that in contrast to the carbon case, all BN tubes are insulators and have a nearly constant quasiparticle band gap of near 5.5 eV independent of diameter and helicity for tubes with $d \geq 10$Å with the bottom of the conduction being a novel free-electron tubule state. The possibility of chiral currents in BC_2N nanotube is investigated. Synthesis of all three types of B-C-N nanotubes have been achieved in recent experiments. The rapid progress in the past four years demonstrates the very richness of this active field. Undoubtedly, discoveries of more new properties and new classes of nanotubes will occur in the future.

Acknowledgments

I would like to acknowledge collaboration with X. Blase, L. X. Benedict, E. Shirley, V. H. Crespi, A. Rubio, Y. Miyamoto and M. L. Cohen and the experimental group of A. Zettl on various parts of the work reviewed here. This work was supported by NSF Grant No. DMR95-20554 and by the U.S. DOE under Contract No. DE-AC03-76SF00098. Supercomputer time was provided by the NSF San Diego Supercomputer Center, the NSF Pittsburgh Supercomputer Center, and by the National Energy Research Supercomputer Center.

References

1. S. Iijima, Nature **354**, 56 (1991).
2. S. Iijima and T. Ichihashi, Nature **363**, 603 (1993); D.S. Bethune et al., Nature **363**, 605 (1993).
3. X. Blase, L.X. Benedict, E.L. Shirley, and S.G. Louie, Phys. Rev. Lett. **72**, 1878 (1994).
4. N. Hamada. S. Sawada, and A. Oshiyama, Phys. Rev. Lett. **68**, 1579 (1992).
5. R. Saito, M. Fujita, G. Dresselhaus, M.S. Kresselhaus, Appl. Phys. Lett. **60**, 2204 (1992).
6. J.W. Mintmire, B.I. Dunlap, and C.T. White, Phys. Rev. Lett. **68**, 631 (1992).
7. S. Sawada and N. Hamada, Solid State Comm. **83**, 917 (1992).
8. L. X. Benedict, S. G. Louie and M. L. Cohen, Phys. Rev. B (in press).
9. M.R. Pederson, A.A. Quong, Phys. Rev. B **46**, 13584 (1992).
10. G.F. Bertsch, A. Bulgac, D. Tomanek, and Y. Wang, Phys. Rev. Lett. **67**, 2690 (1991).
11. B. Koopmans, PhD Thesis, University of Groningen, 1993.
12. M. R. Pederson and J. Q. Broughton, Phys. Rev. Lett. **69**, 2689 (1992).
13. P.M. Ajayan and S. Iijima, Nature **361**, 333 (1993).
14. E. Dujardin, T.W. Ebbessen, H. Hiura, and K. Tanigaki, Science **265**, 1850 (1994).
15. Y. Miyamoto, A. Rubio, X. Blase, M. L. Cohen, and S. G. Louie, Phys. Rev. Lett. **74**, 2993 (1995).

16. A. Rubio, Y. Miyamoto, X. Blase, M. L. Cohen, and S. G. Louie, to be published.
17. H. Zabel, A. Magerl, A.J. Dianoux, and J.J. Rush, Phys. Rev. Lett. **50**, 2094 (1983).
18. D.P. DiVincenzo and E.J. Mele, Phys. Rev. B **32**, 2538 (1985).
19. N. G. Chopra, L. X. Benedict, V. H. Crespi, M. L. Cohen, S. G. Louie, and A. Zettl, to be published.
20. L. A. Girifalco and R. A. Lad, J. of Chem. Phys. **25**, 693 (1956).
21. A. Rubio, J.L. Corkill, and M.L. Cohen, Phys. Rev. B **49** (1994) 5081. We note that large-size turbostratic, tubular BN structures had been previously reported to be obtained upon heating of amorphous BN to 1100 C. See: E.J.M. Hamilton, S.E. Dolan, C.M. Mann, H.O. Colijn, C.A. McDonald, and S.G. Shore, Science **260**, 659 (1993) .
22. X. Blase, A. Rubio, S. G. Louie, and M. L. Cohen, Euro. Phys. Lett. **28**, 335 (1994).
23. Y. Miyamoto, A. Rubio, S. G. Louie, and M. L. Cohen, Phys. Rev. **B50**, 18360 (1994).
24. Y. Miyamoto, A. Rubio, S. G. Louie, and M. L. Cohen, Phys. Rev. **B50**, 4976 (1994).
25. X. Blase, A. Rubio, S. G. louie, and M. L. Cohen, Phys. Rev. **B51**, 6868 (1995).
26. Z. Weng-Sieh, et al, Phys. Rev. **B51**, 11229 (1995).
27. O. Stephen, et al, Science **266**, 1683 (1994).
28. N. G. Chopra, J. Luyken, K. Cherrey, V. H. Crespi, M. L. Cohen, S. G. Louie, and A. Zettl, to be published.
29. P. Gleize, et al, J. Materials Science Letters **13**, 1413 (1994).
30. F. Williame, L. Boulanger, and M. Cauchetier, MRS Fall Meeting 1994.
31. J. Kouvetakis, R. B. Kaner, M. L. Sattler, and N. Bartlett, J. Chem. Soc. Chem. Commun., 1758 (1986).
32. J. Kouvetakis, et al, Synthetic Metals **34**, 1 (1989).
33. M.S. Hybertsen and S.G. Louie, Phys. Rev. Lett. **55**, 1418 (1985); Phys. Rev. B **34**, 5390 (1986).
34. A. Y. Liu, R. M. Wentzcovitch, and M. L. Cohen, Phys. Rev. **B39**, 1760 (1988).
35. Y. Miyamoto, S. G. Louie, and M. L. Cohen, to be published.